Lithographic Evaluation of the EUV Engineering Test Stand

Sang H. Lee[*a], Daniel A. Tichenor[b], William P. Ballard[a], Luis J. Bernardez II[b], John E. M. Goldsmith[b], Steven J. Haney[b], Karen L. Jefferson[b], Terry A. Johnson[b], Alvin H. Leung[b], Donna J. O'Connell[b], William C. Replogle[b], John B. Wronosky[b], Kenneth Blaedel[c], Patrick Naulleau[d], Kenneth A. Goldberg[d], Eric M. Gullikson[d], Henry N. Chapman[d], Stefan Wurm[e], Eric Panning[a], Pei-Yang Yan[a], Goujing Zhang[a], John E. Bjorkholm[a], Glenn D. Kubiak[b], Donald W. Sweeney[c], David Attwood[d], and Charles W. Gwyn[a]

[a]Intel Corporation, 2200 Mission College Boulevard, Santa Clara CA 95052
[b]Sandia National Laboratories, PO Box 969, Livermore CA 94551
[c]Lawrence Livermore National Laboratory, PO Box 808, Livermore, CA 94550
[d]Lawrence Berkeley National Laboratory, One Cyclotron Road, Berkeley, CA 94720
[e]Infineon Technologies North America Corp. 1730 N First Street, San Jose CA 95112

ABSTRACT

Static and scanned images of 100 nm dense features were successfully obtained with a developmental set of projection optics (λ/14 projection optics box or POB 1) and a 500W drive laser laser-produced-plasma (LPP) source in the Engineering Test Stand (ETS). The ETS, configured with POB1, has been used to understand system performance and acquire lithographic learning which will be used in the development of EUV high volume manufacturing tools. The printed static images for dense features below 100 nm with the improved LPP source (500W drive laser) are comparable to those obtained with the low power LPP source (40W drive laser), while the exposure time was decreased by more than 30×. Image quality comparisons between the static and scanned images with the improved LPP source are also presented. Lithographic evaluation of the ETS includes flare and contrast measurements. By using a resist clearing method, the flare and aerial image contrast of POB1 have been measured, and the results have been compared to analytical calculations and computer simulations.

Keywords: Extreme ultraviolet, lithography, laser-produced plasma, flare, aerial image contrast, resist resolution

1. INTRODUCTION

Extreme Ultraviolet Lithography (EUVL) has been demonstrated for printing dense features below 70 nm without using resolution enhancement techniques. Since EUVL has much in common with optical lithography, it is well accepted by integrated circuit (IC) manufacturers as the leading candidate for the next generation lithography technology. Due to relatively low numerical aperture at short operational wavelengths, high-resolution images with relatively large depth-of-focus (DoF) can be obtained for EUVL.

In order to support the commercialization of EUVL, the EUV Engineering Test Stand (ETS)[1] has been developed as an alpha-class tool in the Virtual National Laboratory funded by the EUV Limited Liability Company (LLC). Full-field printing of high resolution EUV images has been demonstrated in both static and step-and-scan mode using low (40W drive laser)[2,3] and high (500W drive laser) power LPP sources. The demonstrated ETS field size of 24 mm by 32.5 mm is the largest high-resolution EUV field printed to date. Ongoing work with the ETS is providing the system learning required to develop commercial EUVL tools. Currently, a developmental set of projection optics, called POB1, is installed in the ETS to understand system performance and acquire lithographic learning which will be used in the development of EUV high volume manufacturing tools. POB1, a 4x reduction projection system, contains 4 multilayer mirrors and has a numerical aperture of 0.1 at the wafer. The wavefront quality[4] of the POB1 is measured to be ~λ/14 rms, and the intrinsic flare[2-3] is ~50%. An improved projection system of the same design, POB 2, has been fabricated with ~λ/20 rms wavefront error[5] and ~20% intrinsic flare. Sub-field imaging experiments at the Advanced Light Source have demonstrated the printing of 70 nm dense features and smaller[6, 7].

* **Correspondence: Email: sang.h.lee@intel.com; Telephone: 408 653 5075; Fax: 408 765 2554**

Emerging Lithographic Technologies VI, Roxann L. Engelstad, Editor
Proceedings of SPIE Vol. 4688 (2002) © 2002 SPIE · 0277-786X/02/$15.00

To meet the EUVL learning objective, the lithographic performance of the ETS was characterized in its initial configuration, which utilized the low power (40W) drive laser for the laser-produced plasma source and POB1. Baseline results subject to these limitations were acquired for comparison to the ETS performance as system improvements continue to be implemented. A number of significant results have been acquired to date with the low power LPP source. The early learning which includes in-situ astigmatism corrections, preliminary flare measurements, and ETS pupil fill effects, have been presented previously[1-3].

Extensive ETS system upgrades have been completed since successful demonstration of the ETS last year. Lithographic evaluation of the ETS continues as the system is upgraded to enhance performance. The main upgrades include wafer and reticle stages improvement, increased EUV source power, and system control improvement[8, 9].

The LPP source upgrade is being achieved in 3 stages using 500, 1000, and 1500 W of TRW laser power, respectively. (The source power upgrade[9] is obtained using a single chain of the 3-chain, 1500 watt, Nd:YAG laser developed by TRW.) The LPP source with a single chain TRW laser is referred as a high power LPP source throughout the paper. Lithographic evaluation with the high power source upgrade is discussed in detail here. The printed static images for dense features below 100 nm with the high power LPP source are comparable to those obtained with the low power LPP source (40W driver laser), while the exposure time was decreased by more than 30×. Scanned images with the high power LPP source are also obtained. The skew and magnification errors must be reduced to one part in 100,000 or less to print high quality scanned images. Image quality comparison between the static and scanned images with the improved LPP source is presented.

More recently, characterization of EUV flare and aerial image contrast have been demonstrated in the ETS using POB1. EUV flare over the entire field is expected to be constant unlike flare in DUV lithographic tools[10]. By using a resist clearing method, a conventional lithographic method, the full-field flare of POB1 has been measured. The lithographically measured flare and calculated flare over the entire arc field have been compared, and good agreement has been achieved confirming that the flare in EUVL is constant over the field. Also, aerial image contrast was characterized in the ETS using a resist clearing method. The experimental results have been compared to computer simulations and analytical calculations, and the aerial image contrast is found to be less than predicted for small feature sizes. The possible sources of discrepancies and the impact of a finite resist resolution on aerial image contrast measurements are discussed.

Further future upgrades in the ETS will improve lithographic performance. Projection optics box #2 (POB 2) with λ/20 rms wavefront quality will be installed in the ETS as a future upgrade[8]. The full power LPP source[9] will be also integrated in the ETS.

2. ETS ILLUMINATION FIELD AND ETS MASK

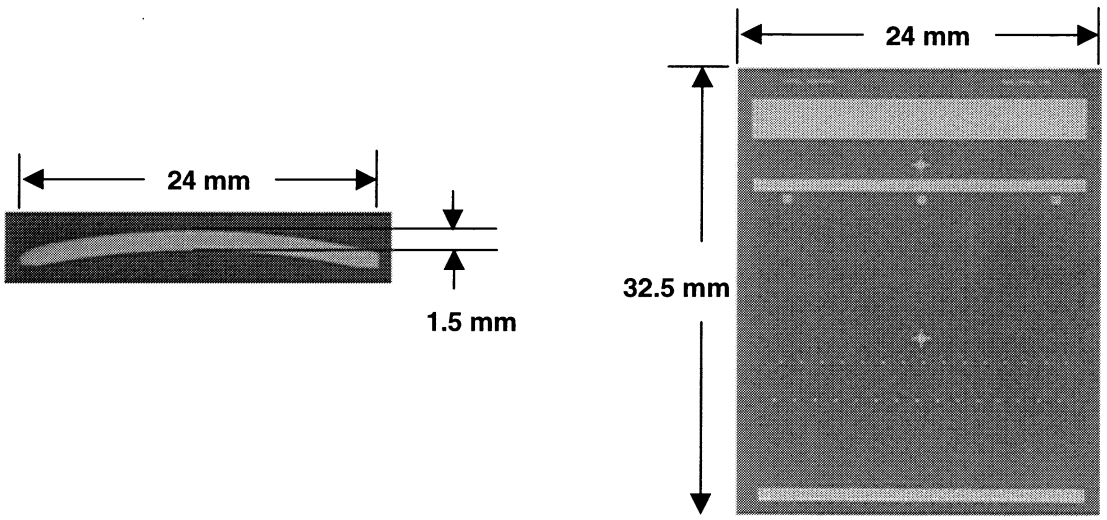

Fig. 1: (a) ETS illuminator provides uniform illumination over a 28° arc shown above. (b) The ETS mask covers the full field in step-and-scan mode. The full field is extended to 32.5 mm in the scanned dimension. The print field size is the largest high-resolution EUV print field demonstrated to date.

The pulsed Nd:YAG laser beam is incident on a liquid xenon-spray target to produce EUV radiation. The target system is a xenon liquid spray jet with a demonstrated conversion efficiency from laser energy to in-band EUV radiation of 0.5% [9]. A six-channel condenser collects radiation from the source and directs it into the projection chamber, where a final condenser element shapes the beam to illuminate the arc-shaped field of view of the projection system. The various condenser elements consist of multilayer mirrors and grazing incidence mirrors which together with a spectral-purity filter (a Zr foil supported by a Ni wire mesh) remove out-of-band radiation and define the bandwidth of the radiation illuminating the EUV mask. The illuminated field of the ETS is described by a 28° arc, 24 mm in cord length and 1.5 mm wide as shown in Fig. 1(a). Operating in step-and-scan mode, the print field of the ETS extends to 32.5 mm in the scan direction. The ETS field of view is the largest high resolution EUV field of view demonstrated to date, and it is large enough for commercial IC manufacture.

A standard 6" square reflective mask is used in the system. The ETS mask printed on a 24 mm by 32.5 mm die site on the wafer is shown in Fig. 1(b). The mask is made with 20 nm thick SiO_2 buffer layer and 70 nm thick Cr absorber layer on a reflective mask blank, and the mask blank is coated with 40 bi-layers of Mo/Si on a ULE substrate. The average EUV reflectivity after fabrication is ~60%. The mask pattern contains a variety of bright field and dark field features designed to characterize imaging performance at feature sizes as small as 50 nm. In current ETS configurations using a 500-watt drive laser, the scan time for full field images is ~4 minutes for 100 nm-thick Shipley EUV 2D baseline resist. The use of all three chains of TRW lasers at the full 1500W will further improve the throughput of the system [8, 9].

3. RECENT ETS LITHOGRAPHIC RESULTS

Characterization of the ETS using PO Box 1 and a low power drive laser (40W) was intended to provide a baseline performance metric to which future results can be compared as major system upgrades are implemented. More recently, static and scanned images with the high power LPP source were obtained, and the results have been compared to the baseline performance. Flare and aerial image contrast have been measured to characterize lithographic performance of the projection optics and resist.

3.1 High power image in the ETS

3.1.1 Static image with a 500W drive laser

Static exposures of 100 nm features using a single 500W chain of the TRW laser have been demonstrated. The static printing has been valuable in characterizing system performance and for in-situ alignment of projection optics [1-3]. By improving the drive laser power from 40W to 500W and the laser plasma target from the Xe cluster jet to the liquid Xe spray jet target, 15× to 30× improvement in exposure time has been achieved [9]. The decrease in exposure time eliminates possible system vibration or drift during the long exposure times required for the low power LPP source [1]. A static image of a 100 nm dense elbow pattern exposed with the high power LPP source is shown in Fig. 2(a). For comparison, a 100 nm elbow pattern using the low power LPP source is shown in Fig. 2(b). No siginificant difference between two images is discernible. The H-V bias, iso-dense bias, and LER values extracted from images such as the one shown in Fig. 2 are due to the quality of the POB1 and mask illumination, and they have been predicted and studied in reference 2 and 3 with aerial image simulation tools.

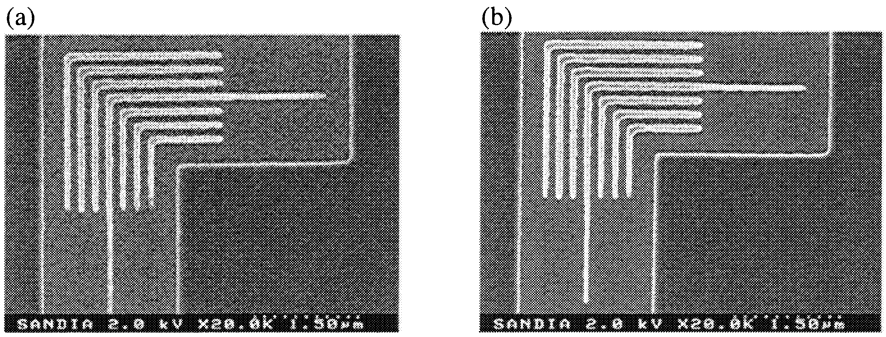

Fig. 2: (a) Static 100 nm image with the 500W drive laser. (b) Static 100 nm image with a 40W drive laser. Exposure time has improved by up to 30× from the low power LPP source to the high power LPP source while maintaining similar printing quality.

3.1.2 Skew and scan magnification

The first scanned images with the ETS were demonstrated last year with the low power LPP source [2, 3]. Lithographic experiments were performed to demonstrate scanned images using the improved LPP source and to validate system changes including the wafer stage and sensor electronics upgrades for high repetition rate. To operate in step and scan mode it is necessary to match scan speed of the wafer stage to that of the reticle stage. Equivalently, the scan magnification, or ratio of wafer-stage to reticle-stage speeds, must match the optical magnification of the projection system. If these parameters are not matched, the horizontal features, which have structure in the scan direction, will be degraded by motion blur (See Fig. 3(a)).

A similar degradation occurs, if the scan direction of the wafer stage is not matched to that of the scanning aerial image. This affect can be stated in terms of stage skew, which is the angle between the scanning axes of the wafer stage and the reticle stage. The stage skew must match the skew between the scan direction of the aerial image and that of the wafer. Skew can be introduced by the projection system or by misalignment between the wafer metrology system and the reticle metrology system. If this parameter is not matched, vertical features, which have structure in the cross-scan direction, will be degraded by motion blur (See Fig. 3(b)).

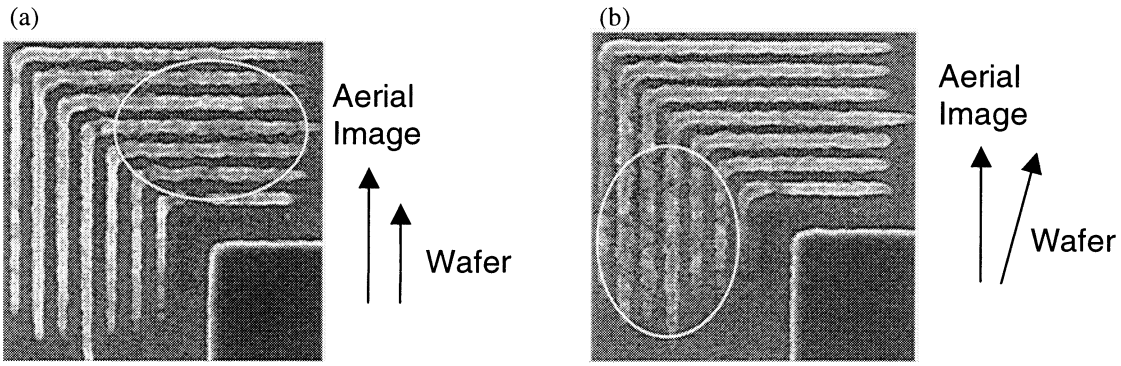

Fig. 3: (a) Scanned image degraded by magnification error, where the reticle and the wafer move at different speeds. (b) Scanned image degraded by skew error, where the reticle and the wafer move in different directions.

To determine the optical magnification, cross-hair marks were printed in resist throughout the ring field. A Leika IPRO tool was used to measure the separation between the marks. These measurements were compared to the known separation of the marks on the reticle. To achieve agreement in the central field region, the optical magnification was 82 ppm greater than the nominal ¼ magnification. This error is within the expected range and easily corrected by adjusting the scan speed ratio. The magnification correction was confirmed by recording images at various scan speed ratios and observing the best result for horizontal features to be at a magnification adjustment of +90 ppm, which is in good agreement with the IPRO measurements.

The determination of skew from printed images of IPRO marks is also possible. This process is complicated by the non-telecentric reticle illumination, which couples reticle roll into the printed location of the IPRO marks. A procedure for extracting skew from a sequence of printed images was developed to support scanned imaging experiments. For these experiments, skew was found by printing images at various skew angles and maximizing the contrast of the dense vertical lines. In a few iterations, the skew was determined to be –210 microradians, which was easily accommodated by the stage range of motion. Using these magnification and skew corrections, the scanned images of 90 nm, 100, and 130 nm dense lines and spaces in two different orientations were printed as shown in Fig. 4. The quality of the 100 nm scanned image (shown in Fig. 4(b)) is indistinguishable from that of the static image (shown in Fig. 2(a)) indicating that the magnification and skew corrections for the scanned images were well established. The wafer stage was operated at the speed of 0.14 mm/sec (reticle stage speed of 0.56 mm/sec).

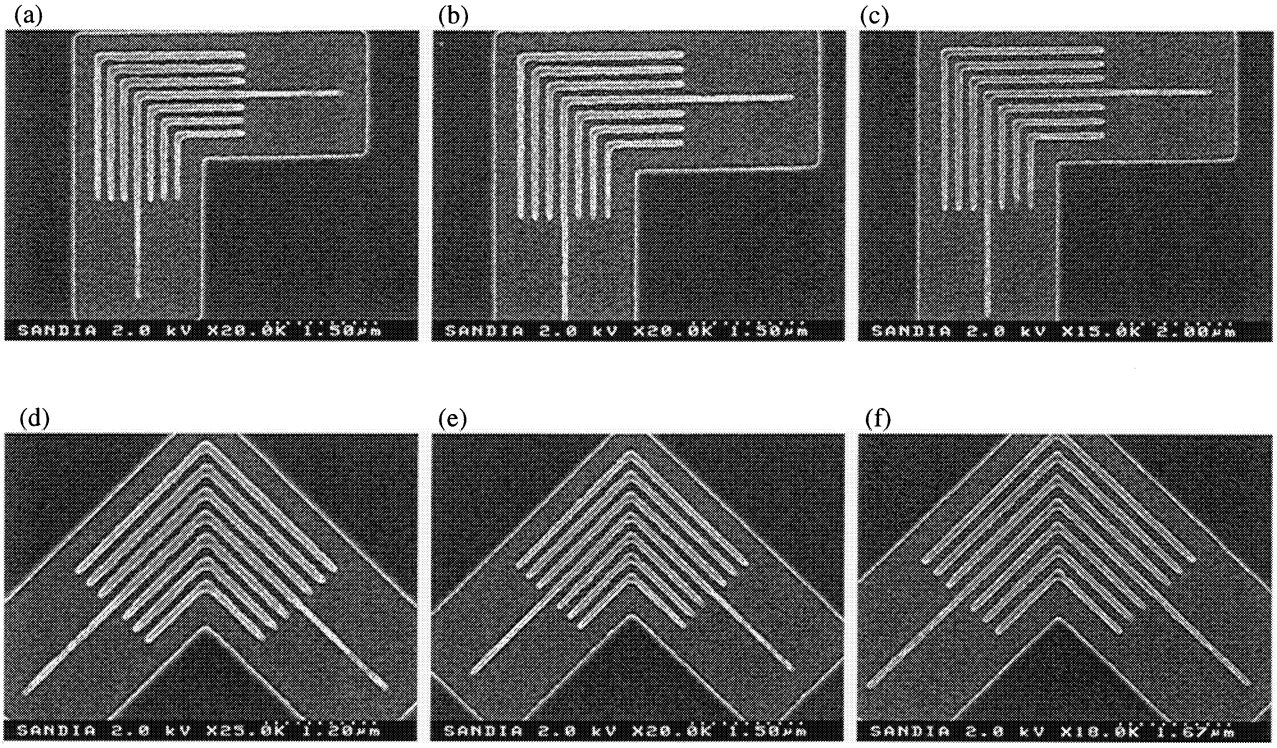

Fig. 4: (a) and (d) Scanned image for 90 nm iso/dense elbows. (b) and (e) Scanned image for 100 nm iso/dense elbows. (c) and (f) Scanned image for 130 nm iso/dense elbows. A magnification correction of +90 ppm and a skew correction of – 210 micro radians were used.

Through-dose and through-focus images of 90 nm dense elbow pattern in scan mode were also obtained. Through-dose images are shown in Fig. 5(a), and through-focus images are shown in Fig. 5(b). The focus was varied by 0.5 μm, and dose was varied by 10%. Approximately 10% exposure latitude with ~1 μm depth of focus (DoF) for ±10 % CD change have been observed for 90 nm dense features in the scanning operation mode.

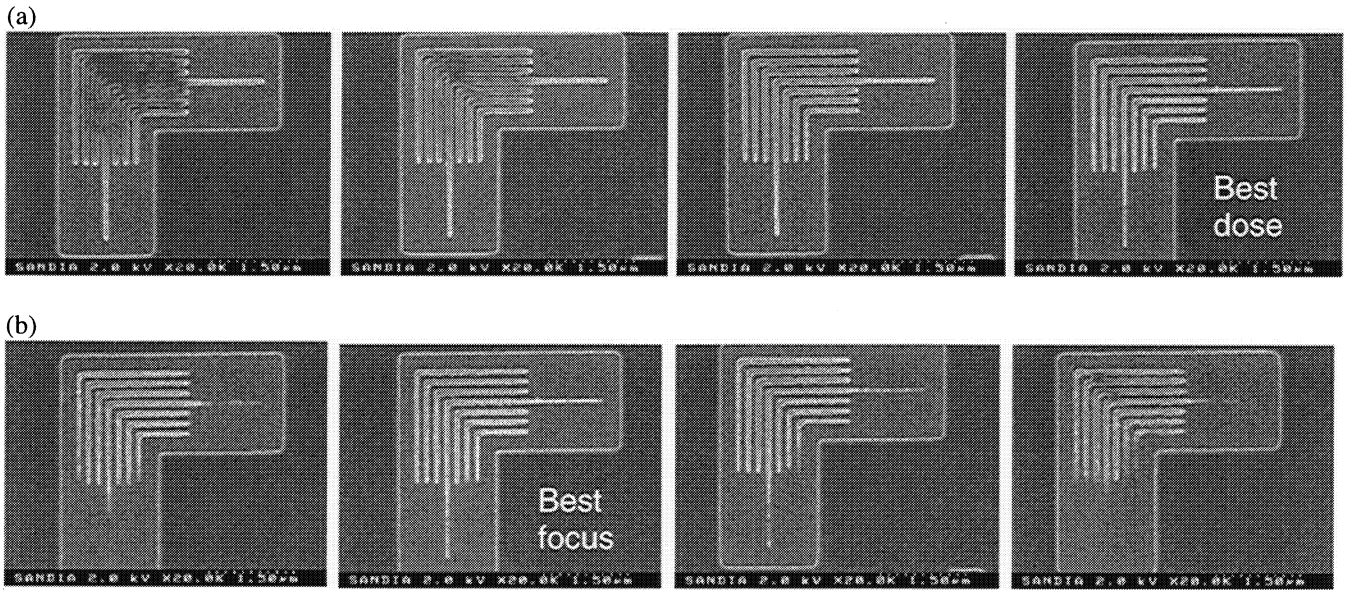

Fig. 5: (a) Through-dose scanned images of 90 nm iso/dense elbows with 10% dose increment are shown. (b) Through-focus scanned images for 90 nm iso/dense elbows with 0.5 μm focus increment are shown.

3.2 Lithographic flare measurements of the PO Box 1

Flare is caused by light scattering from the optical components of a lithography tool system [10, 11]. As the feature size of the printed circuit gets smaller, the importance of flare is also enhanced. Scattering redirects the light from an area of an image intended to be bright into all areas of the image, including those regions intended to be dark. The resulting background illumination within the image field is called flare, and it can reduce image contrast, lead to CD variations, and shrink the process window. Mid-spatial frequency roughness of the imaging mirror surfaces creates the flare.

The magnitude of the flare is proportional to $1/\lambda^2$. Thus, as the wavelength for the lithographic system gets smaller, the effects of flare increases. Since EUV wavelengths are shorter than the conventional DUV wavelengths by an order of magnitude, the amount of flare can be significant [10]. Thus, understanding of the flare contribution to the printed features in EUVL is critical. The EUV flare is simpler than DUV flare because the flare for EUVL is only generated by the rough surfaces of projection optics, while DUV flare can be generated by many components in the lithography tool [10]. The EUV flare on the wafer plane can be calculated if mirror roughness is known. Also, DUV flare has a significant variation over the field, while EUV flare is almost constant over the field, except for the very edges of the field due to short range scattering in EUV [10].

EUV flare can be directly identified by measuring the extended point spread function of the projection system, but it requires a coherent EUV source like a synchrotron [11]. As an alternate method, flare can be lithographically measured by printing dark features in the bright field region. This is also known as the resist clearing method. Lithographic measurement of flare has been performed in the ETS using the improved LPP source. Flare for a given feature size is determined by dividing the dose to clear the bright region, E_0, by the dose to clear the dark feature, E_D.

Seven sets of dark line features, ranging from 1 μm to 8 μm, are located in the bright field region of the mask to measure flare over the entire arc field as shown in Fig. 6. The seven sets of the flare features are evenly spaced out in the arc to cover the entire field. This bright field was exposed onto a wafer with various dose levels at an increment of 10%, until the given dark features disappear completely. The 2 μm line with 1:5 aspect ratio is shown in Fig. 7(a). As the dose approaches E_D, the feature washes out. The flare at the center of the smile field is determined to be ~40% based on the 2 μm line feature. The calculated flare values using the actual power spectral density of the imaging mirror surfaces and the lithographically measured flare values of the PO Box 1 for the 2 μm line feature with 1:5 aspect ratio at seven field points are plotted in Fig. 7(b). The predicted and measured values agree to within the error bar, associated with the coarse dose increments. This error can be reduced by taking finer dose steps. Also, measured flare is constant over the field as expected. Since flare is constant over the field, compensation is possible if needed [10]. The flare is expected to be far less for POB2, an improved set of projection optics, as shown by the calculated flare for POB2 as plotted in Fig. 7(b). The required range of flare for commercial EUV optics is less than 10% [10].

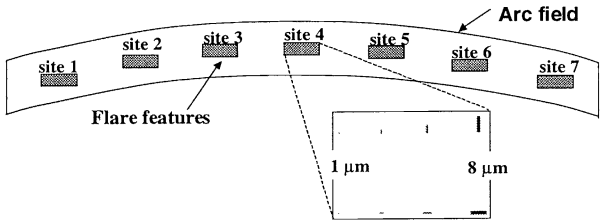

Fig. 6: Seven sets of dark line features, in the size ranging from 1 μm to 8 μm, are located in the bright field region of the mask to measure flare over the entire arc field.

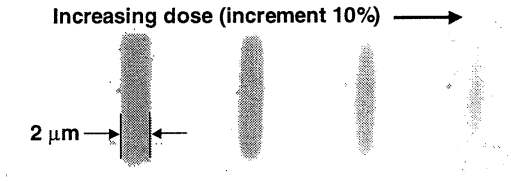

(a)

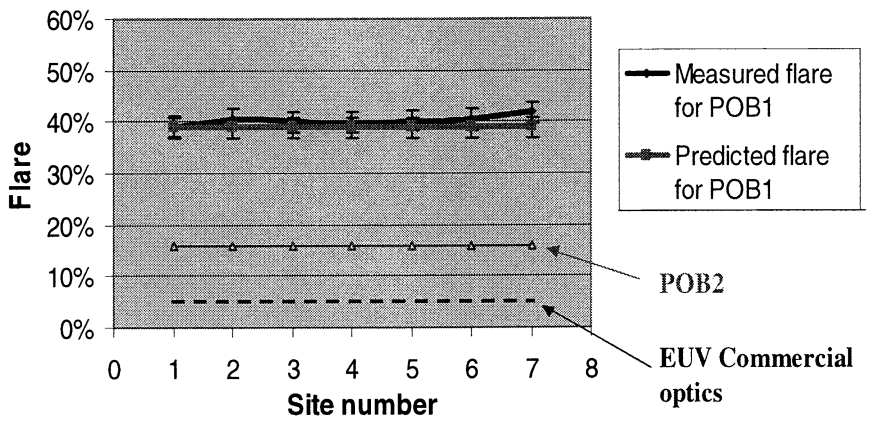

(b)

Fig. 7: (a) Flare features (2um) printed with a 10% dose increment per image from left to right. (b) Flare measured lithographically compared to theory based on mirror roughness.

3.3 Measurement of aerial image contrast in the ETS

POB1 has been valuable in integrating the ETS and understanding system performance. One issue with POB1 is the apparent diminished contrast of aerial images as compared with modeling results for small feature sizes. It is widely understood that the aerial image contrast needs to be at least 50 % or higher for reliable print quality. Aerial image contrast can be used to identify possible system drift and test resist resolution, which affects the printing of high-resolution patterns. The minimum aerial image contrast for vertical and horizontal features printed with POB1 has been experimentally determined by using a resist-clearing method, which is very similar to the one used for the flare measurements in the ETS. This experiment was performed using Shipley's EUV 2D baseline resist process.

The relationship between I_{max} (or I_{min}) and $Dose_{min}$ (or $Dose_{max}$) is described in Fig. 8, and using the resist threshold approximation, the contrast of the printed dense lines is described by the following equation,

$$Contrast = \frac{Dose_{\max} - Dose_{\min}}{Dose_{\max} + Dose_{\min}} \tag{1}$$

$Dose_{max}$ and $Dose_{min}$ for a given feature size can be obtained by analyzing SEM images as shown in Fig. 9. The aerial image contrast can be calculated from Eq. (1).

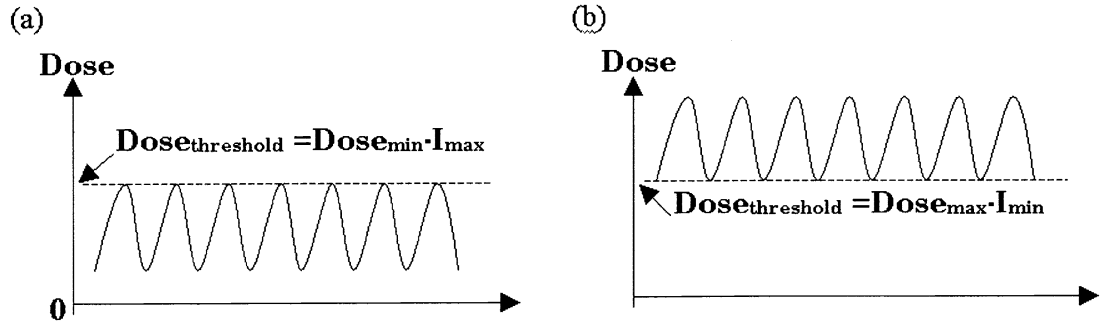

Fig. 8: Resist threshold approximation to obtain the $Dose_{max}$ and $Dose_{min}$. (a) $Dose_{min}$ is a dose level to clear the spaces. (b) Similarly, $Dose_{max}$ is a does level to clear the lines.

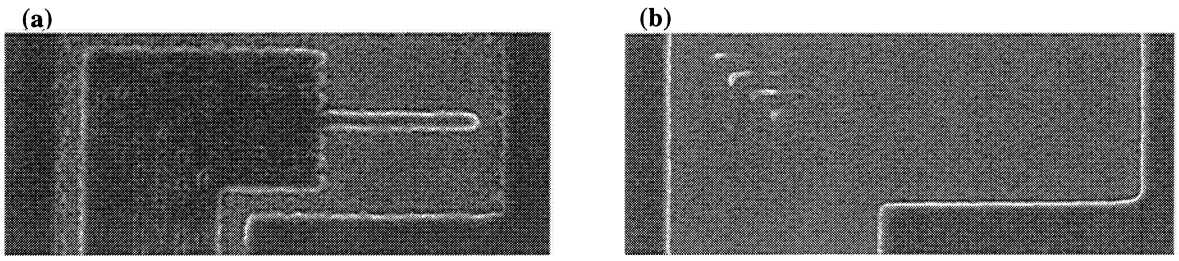

Fig. 9: SEM image analysis to obtain $Dose_{min}$ and $Dose_{max}$. (a) $Dose_{min}$ can be obtained from this lightly dosed image. $Dose_{min}$ is a dose level which just starts to clear the spaces. (b) $Dose_{max}$ is a dose level to clear the lines completely. Using the heavily dosed images, $Dose_{max}$ can be measured.

Intel's I-Photo aerial image simulation tool was used to calculate the theoretical contrast values. The simulation parameters include the 6-channel illumination and the measured raw wavefront data at the central field point. The raw wavefront data accounts for flare covering up to a 14 μm-diameter region around a given field point at the wafer plane. Since the simulated image area is less than 8 μm in diameter, most of the flare is included in the image model.

The measured aerial image contrast was compared with the predicted values from the simulations. The measured aerial image contrast for small dense features is less than the theoretical values as shown in Fig 10. Various potential sources have been identified as the cause for these discrepancies. For example, a better-than-expected wavefront used in the model can overestimate the aerial image contrast; drift or vibration of the wafer and reticle stages can degrade aerial image contrast for long exposed images; and image contrast degradation due to the stage drift would be severe for the smaller features.

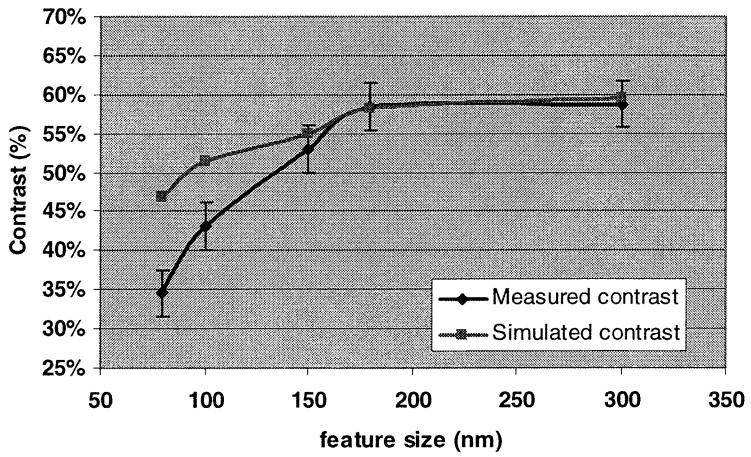

Fig. 10: The plot of theoretical contrast values and measured values. Simulations and experiments are in good agreement for larger features, but discrepancies are observed for small features.

A major source of the discrepancies could be a finite resist resolution. The resist resolution is one of the fundamental limitations to small-feature printing in EUV lithography for a given resist thickness. If the resist resolution is not fine enough to print the desired feature sizes, the contrast of printed images can be lower than the actual aerial image formed by lithographic projection optics. Exposure of a single point on the resist would produce a spot of finite diameter. This spot represents the point-spread function (PSF) of the resist. The resist behavior is described by an empirical model in which the aerial image is convolved with the resist PSF, and the resist contrast curve is applied to the result. If the PSF of EUV 2D were 50 nm in diameter, it would have a similar effect on the resulting image as the stage drift. The major difference is that the resist PSF would cause an isotropic degradation, while unidirectional drift should degrade lines in one orientation

only and not degrade those perpendicular to that direction. A non-degraded direction in the contrast-wafer images could not be identified.

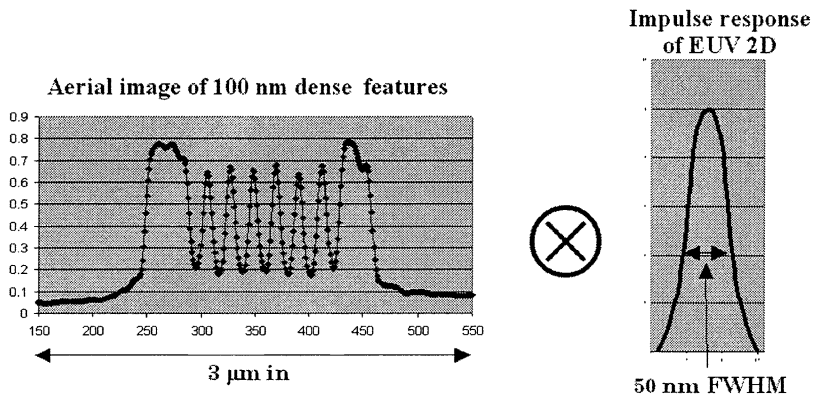

Fig. 11: An example of calculating printed images with the resist behavior. A simulated aerial image is convolved with the impulse response of the resist. The resulting image represents the final image printed on resist. This is a simple model to account for the finite resist resolution.

Simulated aerial images of 100 nm dense features have been convolved with the PSF using MATLAB as illustrated in Fig. 11 to simulate the effect of the finite resist resolution. The resist contrast has been assumed to be a step function. With a few iterations, a 50 nm FWHM PSF has been found to be reasonable and fit well to the experimental results. Using the same method, image contrast has been recalculated for various feature sizes, and the experimental values are plotted with the newly calculated values in Fig. 12. Good agreement is observed between simulations and calculations, especially for 80 nm features. A similar result has also been observed for POB 2 currently operating in the Static Exposure Station (SES) at the ALS. Evidence points strongly to the finite resolution of the resist as being the primary cause of the discrepancy shown in Fig. 10.

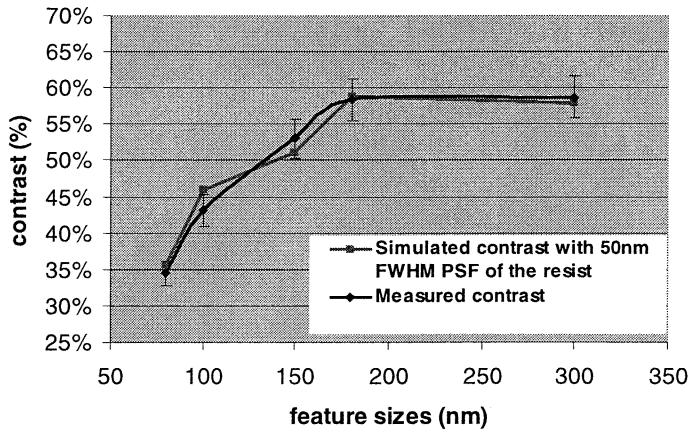

Fig. 12: Using the method described in Fig. 11, aerial image contrast has been recalculated for various feature sizes, and the experimental values are plotted with the calculated value. As shown here, good agreement is observed between simulations and calculations, especially for 80 nm features.

Other sources of discrepancy include the 5 % dose steps, out-of-band radiation, a non-linear resist contrast for small features, and illuminator degradation. As shown in Fig 9, the $Dose_{max}$ and $Dose_{min}$ were measured based on the SEM images. A maximum error from evaluating the SEM images of about ±5 % is assumed due to the subjective factors involved. The EUV 2D resist is based on the DUV resist, and it is sensitive to the DUV wavelengths. Therefore, out-of-

band radiation could have a significant impact on the observed contrast. Currently out of-band radiation is being quantified and the first results indicate that it is not a major factor in the experiments reported here. Resist contrast was assumed to be a step function in the resist resolution analysis described above. The contrast of the resist may not be a perfect step function, so the resist threshold approximation may fail for the small features. The ETS illuminator consists of 6 overlapping channels at the mask plane. If any of the channels are partially blocked in the beam path, the image can be degraded. Further simulations are required to understand those issues.

4. SUMMARY

The ETS has demonstrated the capability to print 100 nm features in both static mode and step-and-scan mode. This result was achieved using a developmental projection system, POB1, and a 500W drive laser for the plasma source. Lithographically measured flare in POB1 is constant across the full arc field and in good agreement with the predicted values. Aerial image contrast of POB1 has been lithographically measured using a resist clearing method. Finite resist resolution can account for the discrepancies between the experiments and simulations. Aerial image contrast measurements indicate the possible limitation of the current baseline resist and suggest that higher resolution resist will be required to reliably print features smaller than 50 nm. Substantial performance improvements in the ETS are expected, when the full power 1500W LPP source and POB2 are integrated into the ETS for application in the EUVL user facility.

ACKNOWLEDGMENTS

The authors are indebted to the members of the subsystem and technology teams, whose hard work is responsible for advancing the EUV Engineering Test Stand to the state of development reported in this paper.

This work was performed by the University of California Lawrence Livermore National Laboratory under the auspices of the U.S. Department of Energy, Contract No. W-7405-ENG-48, by Sandia National Laboratories under the auspices of the U.S. Department of Energy, Contract No. DE-AC04-94AL85000, and by the Lawrence Berkeley National Laboratory under the auspices of the U.S. Department of Energy Office of Basic Energy Sciences. Funding was provided by the Extreme Ultraviolet Limited Liability Company under a Cooperative Research and Development Agreement.

EUVL technology development is funded by the EUV Limited Liability Company (LLC), a consortium of semiconductor manufacturers founded in 1997 and comprised of Advanced Micro Devices, Infineon, Intel, IBM, Micron, and Motorola. The Department of Energy Virtual National Laboratory, comprised of Lawrence Berkeley National Laboratory, Lawrence Livermore National Laboratory and Sandia National Laboratories, perform research, development, and engineering to accelerate the commercialization of EUVL.

REFERENCES

1. D. A. Tichenor, A. K. Ray-Chaudhuri, W. C. Replogle, R. H. Stulen, G. D. Kubiak, P. D. Rockett , L. E. Klebanoff, K. L. Jefferson, A. H. Leung, J. B. Wronosky, L. C. Hale, H. N. Chapman, J. S. Taylor, J. A. Folta, C. Montcalm, R. Soufli, E. Spiller, K. Blaedel, G. E. Sommargren, D. W. Sweeney, P. Naulleau, K. A. Goldberg, E. M. Gullikson, J. Bokor, P. J. Batson, D. T. Attwood, K. H. Jackson, S. D. Hector, C. W. Gwyn, and P. Y. Yan, "System Integration and Performance of the EUV Engineering Test Stand," *Emerging Lithographic Technologies V*, Proceeding of SPIE vol. 4343, p. 19-37 (2001).

2. H. N. Chapman, A. K. Ray-Chaudhuri, D. A. Tichenor, W. C. Replogle, R. H. Stulen, G. D. Kubiak, P. D. Rockett , L. E. Klebanoff, D. O'Connell, A. H. Leung, K. L. Jefferson, J. B. Wronosky, J. S. Taylor, L. C. Hale, K. Blaedel, E. Spiller, G. E. Sommargren, J. A. Folta, D. W. Sweeney, E. M. Gullikson, P. Naulleau, K. A. Goldberg, J. Bokor, D. T. Attwood, U. Mickan, R. Hanzen, E. Panning, P.-Y. Yan, C. W. Gwyn, and S. H. Lee, "First Lithographic Results from the EUV Engineering Test Stand," submitted to J. Vac. Sci. B19, 2389-2395 (2001).

3. D. A. Tichenor, A. K. Ray-Chaudhuri, S. H. Lee, H. N. Chapman, W. C. Replogle, K. W. Berger, R. H. Stulen, G. D. Kubiak, L. E. Klebanoff, J. B. Wronosky, D. J. O'Connell, A. H. Leung, K. L. Jefferson, W. P. Ballard, L. C. Hale, K. Blaedel, J. S. Taylor, J. A. Folta, E. Spiller, R. Soufli, G. E. Sommargren, D. W. Sweeney, P. Naulleau, K. A. Goldberg, E. M. Gullikson, J. Bokor, D. T. Attwood, U Mickan, R. Hanzen, E. Panning, P. Y. Yan, J. E. Bjorkholm, and C. W. Gwyn, "Initial results from the EUV Engineering Test Stand," *Soft X-Ray and EUV Imaging Systems II*, Proc. of SPIE vol. 4506, 9-18 (2001)

4. K. A. Goldberg, P. Naulleau, P. Batson, P. Denham, E. H. Anderson, H. Chapman, J. Bokor, "Extreme ultraviolet alignment and testing of a four-mirror ring field extreme ultraviolet optical system," Journal-of-Vacuum-Science-&-Technology-B-(Microelectronics-and-Nanometer-Structures), vol.18, no.6; Nov. 2000; p.2911-15, (2000).

5. P. Naulleau, K. Goldberg, E. Anderson, P. Batson, P. Denham, S. Rekawa, and J, Bokor, "At wavelength characterization of the Engineering Test Stand Set-2 optic," J. Vac. Sci. & Technol. B19 2396-2400 (2001).

6. P. Naulleau, K. Goldberg, E. Anderson, P. Batson, P. Denham, S. Rekawa, and J. Bokor, "Adding static printing capabilities to the EUV phase-shifting point diffraction interferometer," *Emerging Lithographic Technologies,* Proceedings of the SPIE Vol. 4343 (2001).

7. P. Naulleau, K. A. Goldberg, E. H. Anderson, D. T. Attwood, Jr., P. J. Batson, J. Bokor, P. Denham, E. M. Gullikson, B. Hoef, K. H. Jackson, S. Rekawa, F. Salmassi, K. L. Blaedel, H. N. Chapman, L. C. Hale, R. Soufli, E. A. Spiller, D. W. Sweeney, J. S. Taylor, C. C. Walton, G. F. Cardinale, A. K. Ray-Chaudhuri, A. Fisher, D. J. O-Connell, R. H. Stulen, D. A. Tichenor, C. W. Gwyn, P. Yan, and G. Zhang, "Static microfield printing at the Advanced Light Source with the ETS Set-2 optic," *Emerging Lithographic Technologies,* Proceedings of the SPIE Vol. 4343, pg. 639-645 (2001).

8. D. A. Tichenor, W. C. Replogle, S.H. Lee, W. Ballard, G. D. Kubiak, P. D. Rockett , L. E. Klebanoff, J. E.M. Goldsmith, J. B. Wronosky, L. C. Hale, H. N. Chapman, J. S. Taylor, P. Naulleau, K. A. Goldberg, "Performance Upgrades in in the EUV engineering test stand,' submitted to Proceeding of SPIE vol. 4688, will be published (2002).

9. W.P Ballard, Luis J. Bernardez II, R. Lafon, Y. Perras, R.J. Anderson, A. Leung, H. Shields, M. Petach, R. St. Pierre, R. Bristol, "High-Power Laser-Produced-Plasma Source," *Emerging Lithographic Technologies,* submitted to Proceeding of SPIE vol. 4688, (2002).

10. C. Krautschik, M. Ito, I. Nishiyama, S. Okazaki, "Impact of EUV Light Scatter on CD Control as a Result of Mask Density Changes," *Emerging Lithographic Technologies V*, Proceeding of SPIE vol. 4688, will be published (2002).

11. E. Gullikson, S. Baker, J. E. Bjorkholm, J. Bokor, K. A. Goldberg, J. E. M. Goldsmith, C. Montcalm, P. Naulleau, E. Spiller, D. G. Stearn, J. S. Taylor, J. H. Underwood, "EUV scattering and flare of 10x projection cameras," Proceedings-of-the-SPIE --The-International-Society-for-Optical-Engineering. vol.3676, pt.1-2, p.717-23 (1999).